Characterizing Photovoltaic Backsheet Adhesion Degradation using the Wedge and Single Cantilever Beam Tests, Part I: Field Modules

Scott E. Julien[a], Michael D. Kempe[b], Joshua J. Eafanti[b], Joshua Morse[b], Yu Wang[c], Andrew Fairbrother[d], Sophie Napoli[e], Adam W. Hauser[e], Liang Ji[f], Gregory S. O'Brien[e], Xiaohong Gu[d], Roger H. French[c], Laura S. Bruckman[c], Kenneth P. Boyce[f], Kai-tak Wan[a,*]

[a]*Mechanical & Industrial Engineering, Northeastern University, Boston, MA 02115, USA*
[b]*Photovoltaics Research, National Renewable Energy Laboratory, Golden, CO 80401, USA*
[c]*Case Western Reserve University, Department of Materials Science & Engineering, 10900 Euclid Avenue, Cleveland, OH 44106, USA*
[d]*Engineering Laboratory, National Institute of Standards & Technology, Gaithersburg, MD 20899, USA*
[e]*Arkema, Inc., 900 First Ave., King of Prussia, PA 19406, USA*
[f]*Renewable Energy, Underwriter's Laboratories Inc., Northbrook, IL 60062, USA*

Abstract

Photovoltaic backsheets are exposed to harsh outdoor weathering conditions throughout their service lives that can compromise their protective function through adhesive debonding between their constituent layers and between the backsheet and the module. A large-scale study on adhesive degradation was conducted on 37 field-exposed modules, that spanned 19 different module manufacturers, were deployed among six Köppen-Geiger climatic zones, and were fielded between 0 and 28 years. Six outer layer polymer classes were identified among the backsheets: polyamide (PA), polyethylene terephthalate (PET), polyvinyl fluoride (PVF), polyvinylidene fluoride (PVDF), fluoroethylene vinyl ether copolymer (FEVE), and tetrafluoroethylene/hexafluoropropylene/vinylidene fluoride copolymer (THV). Two adhesion tests were used to measure the adhesive strength: the wedge test and the width-tapered single-cantilever beam

*Correspondence to: Department of Mechanical and Industrial Engineering, Northeastern University, 360 Huntington Ave, SN 334, Boston, MA 02115. Tel: +1 617 373 2248. Fax: +1 617 373 2921

Email address: k.wan@northeastern.edu (Kai-tak Wan)

Preprint submitted to Solar Energy Materials and Solar Cells *October 22, 2019*

(SCB) test. Adhesion energies were compared across exposure time and Köppen-Geiger climatic zone. Many of the PET-, PVF-, and PVDF-based backsheets experienced degradation of the adhesive layer between the backsheet outer and core layers. A consistent trend of decreasing adhesion energy with exposure time was observed in five out of the six backsheet types, Trends among adhesion energy and climatic zone, while expected, were not observed, possibly due to broad ranges in temperature, humidity, and precipitation defining Köppen-Geiger climatic zones. The cantilever beam measurements produced an upper cutoff of approximately 100 J/m^2, above which no modules exhibited field delamination. These results are part of a two-part study quantifying adhesion in both field-weathered and indoor-exposed PV backsheets.

Keywords: backsheet, adhesion, delamination, degradation, field module, photovoltaic

---

1. Introduction

Photovoltaic (PV) backsheets are multilayered polymer sheets laminated to the backside of a PV module that provide electrical insulation, prevent liquid moisture ingress, reflect light to the cells, and protect against mechanical damage. After prolonged exposure to harsh outdoor elements—high levels of temperature, humidity, and ultraviolet (UV) radiation—debonding within the backsheet, and between the backsheet and adjacent layers, can occur [1, 2, 3, 4, 5, 6]. In addition to being a safety hazard, the resulting interlayer voids diminish heat dissipation, leading to hot spots; reduce the effectiveness of the backsheet as a physical barrier; and may serve as collection sites for moisture, accelerating corrosion of metallic internal components [1]. There is a need within the PV community for methods to effectively quantify the adhesive integrity of the backsheet, to allow prediction of adequate performance for the lifetime of a module and allow comparison of one backsheet to another.

Peel tests [7, 8, 9] are the most common method used to assess the adhesive strength of backsheets [10, 11] and encapsulants [11, 12, 13]. Unfortunately, this

method gives results that are difficult to compare across materials. Plastic extension [12] or failure of the peel handle and high angles at the debond front, confound direct measurement of the adhesion energy by introducing large secondary energy dissipation modes. The results of peel tests, consequently, depend strongly upon the material properties (e.g. yield stress) of the peel test sample construction.

Shear tests, such as the lap shear test [14, 15], compressive shear test [16], and rotational torque test [17, 18], have also been used to characterize adhesion in PV systems. However, such tests often lead to significant bulk deformation of the polymer layers and unintended, unrepresentative stress concentrations, leading to results that are highly dependent upon their elastic and plastic properties. More recent testing methods have been developed to minimize such phenomena. Double cantilever beam (DCB) [19], single cantilever beam (SCB) [4, 20, 21], and wedge [22] tests have been used with success in characterizing the adhesive strength in modules and module materials. By adhering a flexible, semi-rigid material to one or both sides of the sample, plastic deformation of the material can be minimized and debonding can occur at relatively low debond angles, to better represent what is seen in the field. Furthermore, by optimizing the mechanical properties of the beam, the mechanical stress can be concentrated near the debond front, reducing secondary bulk material deformation and energy dissipation. These advantages allow a fracture mechanics model to be applied, enabling a critical adhesion energy to be extracted. While not wholly independent of sample geometry (e.g. the encapsulant thickness affects the fracture toughness measurement [5] and the size of the cohesive zone depends on the beam thickness), these tests are still better able to probe adhesion than the others. The failure geometry is better controlled and reproduced, and the mechanics of debonding better duplicate what happens in the field, allowing for better comparison across different backsheet materials.

In addition to these advantages, cantilever beam methods can be used on fielded PV modules to investigate relevant degradation parameters. For peel

tests, the backsheet must still be intact to perform the test, and lap sheer tests generally require engineered samples because the glass is prone to breakage during testing. Cantilever beam tests also allow multiple interfaces to be probed sequentially by debonding one interface and adhering another beam to the same area to probe the next interface. Furthermore, for the wedge test, the debonding can happen at very slow rates that better mimic what happens in a PV module, more easily probing the debonding threshold energy release rate and providing more relevant information.

2. Materials and Methods

2.1. Sample Procurement

A total of thirty-seven (37) modules were retrieved from the field over the course of a three-year project. The study encompassed not only adhesive failure, but other modes of backsheet degradation, including outer layer yellowing and chalking and through-thickness cracking. Modules were specifically selected that: (i) showed one or more of these modes of degradation; (b) were counterparts to some of the degraded modules with similar make, model, or composition, but fielded under different conditions (region, climatic zone, ground cover, etc.); or (c) were unexposed counterparts. Because of this, the resulting set of modules does not necessarily represent the proportions of makes, models, constructions, climatic zones or other module characteristics in field service, today.

Overall, the modules spanned 19 different module manufacturers, field exposure times of 0 to 28 years, and six different Köppen-Geiger climatic zones, five countries, and three continents (see Supplemental Information, SI Table 1). The modules had been exposed under a variety of different ground covers such as grass, rooftop (white and cement), and soil. The outer backsheet layer of each module was identified using Fourier-transform infrared spectroscopy (FTIR). Among the 37 different modules, six different backsheet outer layer polymer classes were identified: polyamide (PA), polyethylene terephthalate (PET), polyvinyl fluoride (PVF), polyvinylidene fluoride (PVDF), fluoroethylene vinyl

ether copolymer (FEVE), and polytetrafluoroethylene/hexafluoropropylene/vinylidene fluoride copolymer (THV). In addition, the cross-sectional layering of each backsheet was identified by sectioning and polishing, followed by Raman spectroscopy.

Adhesion tests were conducted either on the backside of intact, whole modules, or on module sections, cut using a diamond saw. Because the cutting process caused the tempered module front glass to shatter, adhesion of a rigid backing plate to the glass was necessary, to restore rigidity to the portion of the section from which the test coupon would be cut. All of the wedge tests were conducted on such coupons; many (but not all) of the SCB tests were conducted on intact modules. The results of adhesion tests did not depend upon whether the test was conducted on a coupon or an intact module.

2.2. Wedge Test Methodology

Figure 1a illustrates the wedge test. A top beam, with a Young's modulus, E, thickness, t, and width, b, is adhered to the film stack on the backside of a module or coupon. A pre-crack is first initiated in a layer or interface of interest within the film stack. A wedge of known thickness, h, is subsequently inserted and driven along the debonded portion, advancing the debond front. By measuring the distance from the wedge to the debond front (i.e. the "debond length"), c, at incremental positions of the wedge, multiple redundant measurements of the adhesion energy (i.e. the critical strain energy release rate) of the debonding interface, G_c, can be obtained from

$$G = \frac{3}{8} E t^3 h^2 \frac{1}{c^4} \tag{1}$$

Equation (1) is a classic result [23] derived from Euler-Bernoulli beam theory and fracture mechanics, using following assumptions:

(i) the beam is linearly elastic
(ii) deflection of the beam occurs at small angles relative to the substrate
(iii) the substrate and beam do not plastically deform or yield
(iv) the debond front is clearly defined (i.e. any cohesive zone is negligible in length)

(v) any shear stresses between the beam and substrate are negligible

Assumption (iv) is an idealization. In reality, the polymer layers that remain adhered to the substrate and beam undergo both elastic and plastic deformation in the vicinity of the debond front, leading to a non-negligibly large cohesive zone and dependence on sample geometry. This also causes inaccuracy in the measurement of *c*, and is a challenge for all PV adhesion testing methods that rely upon this measurement. In the present work, this error was minimized as

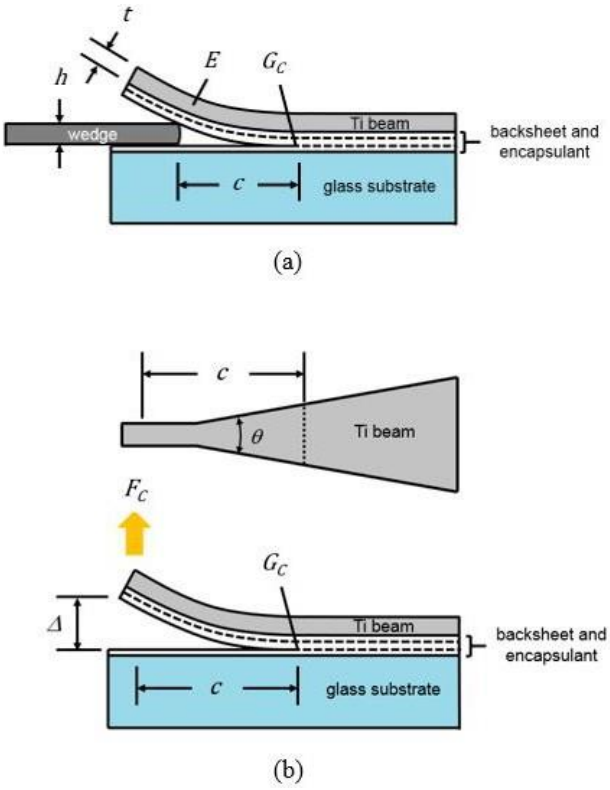

Figure 1: Schematics of the wedge test (a) and width-tapered single cantilever beam (SCB) test (b), with h, the wedge thickness, E, the Young's modulus of the beam, t, the beam thickness, θ, the taper angle (for the SCB beam), c, the debond length, F_c the critical applied force, Δ the crack opening displacement, and G_c, the adhesion energy of the debond interface.

much as possible through careful measurement of c, and the error is included in the uncertainties for G_c reported in the results.

Wedge test coupons were made by first adhering a 6.35-mm (1/4-in) thick rigid aluminum backing plate (50 mm x 75 mm in width and height) to the glass side of a small area of a module section (c.f. Fig. 2a). A two-part epoxy was used (Devcon® 5-Minute Clear Epoxy Resin) to adhere the two. The surfaces were both lightly cleaned with isopropyl alcohol (IPA), prior to assembly. After curing at room temperature, the area was cut away from the module section, forming a test coupon (Fig. 2b).

For beam material, grade 5 (6AL-4V) titanium alloy (Ti) was chosen because of its high ratio of yield strength to Young's modulus. The beams were of a uniform 5-mm width, and a thickness of 0.43 mm was chosen to maximize deflection angle while avoiding yielding during testing. To prepare the backsheet for adhering the beams, the surface was cleaned thoroughly with IPA, sometimes accompanied by a light sanding with fine-grit sandpaper. In cases where the backsheet outer layer was particularly difficult to adhere to—as was com- monly the case with PET—a handheld corona plasma treater (Electro-Technic Products®, Chicago, IL, USA) was used to functionalize the surface. This treatment method is low-temperature and only penetrates to a depth of several nanometers [24]. As such, it was not considered as having an impact on the adhesion test results when debonding occurred more than several nm from the backsheet surface. A cyanoacrylate ("CA", Loctite® 495) or a two-part methacrylate adhesive (3M® DP 8005) was used to bond the beams to the backsheet. A typical layering structure of the final, resulting coupon is shown in Fig. 2c.

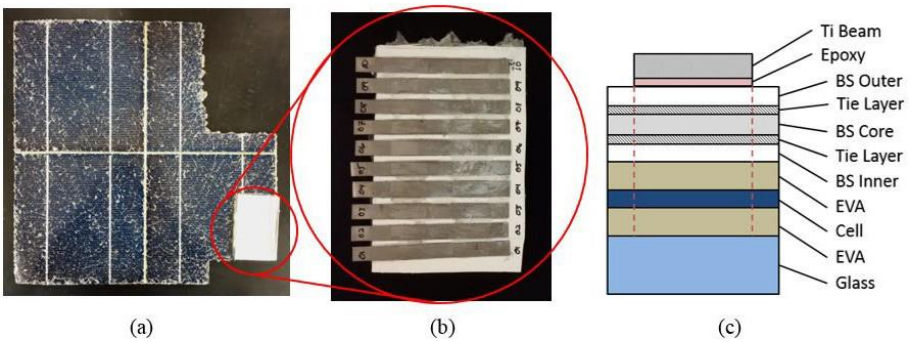

Figure 2: Construction of a wedge test sample from a field-retrieved module: (a) aluminum backing plate adhered to the broken glass-side of a PV module section; (b) titanium (Ti) test beams adhered to the backsheet outer layer of the resulting coupon; (c) resulting layering structure of the coupon, with vertical dashed lines indicating the pre-cuts through the film stack.

To conduct a test on a beam, a razorblade is used to cut around the periphery

of the beam, down to the glass. A pre-crack is subsequently generated in a pre-selected layer or interface in the film stack. While this creates a preference for initial debonding there, the debond interface eventually often migrates to the weakest layer or interface.

In the present study, a wedge of 1.23 mm thickness and 5 mm width was used. After inserting it into the pre-crack, the entire assembly was mounted in a linear actuator, and the wedge was driven in increments of 1-2 mm, at a rate of 1 mm/s. Testing was conducted at laboratory ambient conditions (23±2°C, 15-45% RH). While it has been shown that an increase in in situ relative humidity from 20% to 60% can decrease the measured interlaminar adhesion energy in a backsheet by as much as 25% [20],[i] it was not possible to perform controlled humidity testing during the present study, due to the large volume of samples that required testing. Also of note is that study was that there seemed to be a step change around 50% RH. Considering this, we anticipate that the lack of humidity control results in relative contributions to uncertainty less than 25%. At each wedge position, the assembly was held fixed for 10-20 seconds while the debond length was being measured. This dwell time likely resulted in some slight additional propagation of the debond front, as debonding in PV adhesion tests is known to be time-dependent [20, 21]. It should be noted, however that it is not on the order of that which occurs in field modules (months to years), and therefore likely produces shorter debond lengths and higher adhesion energies. To measure the debond length, the debond front was located using a combination of optical observation and acoustic tapping. In the latter, an instrument was used to tap on the beam, and the front was identified by a distinct change in acoustic resonance. Between five and twelve debond lengths, on average, were measured for each beam, until a typical sample size of 15-20 redundant measurements was obtained. Equation (1) was then used to calculate the adhesion energy corresponding to each debond length, and the mean and first standard deviation of these were reported.

2.3. Tapered Single Cantilever Beam (SCB) Methodology

The tapered single cantilever beam (SCB) test [25] is depicted in Fig. 1b. As

in the wedge test, a beam of elastic material—such as titanium (Ti) or poly methyl methacrylate (PMMA)—is adhered to the outer layer of the backsheet. A pre-crack is initiated at a location of interest, and the beam is then loaded at its end with a vertical applied force, F, and crack opening displacement, Δ, while being pulled at a constant displacement-controlled rate, $d\Delta/dt$. The beam is of a tapered geometry, such that the relationship between the adhesion energy, G_c, and critical applied load, F_c, is theoretically constant for small displacements

where simple beam theory applies [4, 5, 20, 21]

$$G_c = \frac{F_c \quad \Delta}{2tan(\theta/2)\ c^2} \tag{2}$$

For the beam, a thickness of 0.82-mm titanium grade 5 was selected to maximize deflection angle while avoiding yielding during testing. The beam was cut using water jet cutting to dimensions according to IEC TS 62788-6-3 Ed. 1 [25], which uses an angle of 20° for the wedge with the hole for mounting the loading tab at the point where the apex of the beam would be, if not for the rectangular end. The procedure for adhering a backing plate to the front-glass (when necessary), and for adhering the SCB beams to the backsheet, was the same as that for the wedge samples, using 3M® DP 8005 epoxy adhesive.

To conduct an SCB test, the beam was cut around its periphery and a pre-crack was generated in the same manner as in the wedge test. The load- ing tab was connected to a portable loading frame with a 220-N load cell (Delaminator®, DTS, Menlo Park, CA, USA) using a clevis joint with a sapphire jewel bearing of inner radius, 0.5 mm, and outer radius, 1.5 mm, for use with a 1-mm loading pin. The frame was positioned such that the linkage was maintained in as vertical a position as possible throughout the duration of the test, to minimize non-vertical forces during testing. Testing was performed at a displacement-controlled rate of 10 μm/s. Testing was conducted at 23±2°C and 25-70% RH. For each test, the beam was pulled until delamination had progressed sufficiently to produce a distinct delamination plateau in the force-displacement curve, corresponding to the critical applied load, F_c. The final debond length, c, and crack opening displacment, Δ, were measured and used, together with F_c and the known properties of the beam, to calculate G_c from (2). To compute the error for the SCB test, the method specified by IEC TS 62788-6-3 [25]—which only includes the uncertainty in the measurement of F_c—was adapted to include the uncertainty in the measurement of c. The latter was the most error-prone measurement in the tests and was estimated to be ±10%. (The

uncertainties in F_c and Δ, by comparison, were estimated to be <5% and <1%, respectively. The latter was considered negligible for practical purposes.)

3. Results and Discussion

All thirty-seven (37) modules were tested using the wedge test, while twenty-six (26) were tested using the SCB test. The results are given in Figs. 3-9, grouped according to backsheet outer layer type. Fig. 3 corresponds to the

modules with PA-based backsheets; Fig. 4 to the PET-based; Fig. 5 to those PVF-based backsheets with a PVF inner layer; Fig. 6 to those with an EVA or other inner layer; Fig. 7 to the PVDF-based backsheets; Fig. 8 to the FEVE-based; and Fig. 9 to the THV-based. When known, the module manufacturer, backsheet layering composition, deployment location, Köppen-Geiger climatic zone identifier and descriptor, and years of exposure, are provided. To protect the commercial interests of the module manufacturers, however, their names have been anonymized into single-letter identifiers. Occasionally, some of the characteristics of a module were unknown, as indicated by a blank field or '???'. In addition, during testing, some samples debonded at an identifiable interface, but their adhesion energy was not measured, typically because it was too low for the testing method to capture. One module (6) debonded at an interface that was not identified after testing.

3.1. Comparison between Testing Methods

A comparison of the adhesion energy values between the wedge test and SCB test, for those modules that failed at the same interface in both, generally shows that the energy values for the wedge test tended to be higher than for the SCB test, although they were not always statistically significantly so. One reason for this was the shallower angle of deflection of the beam in the wedge test, due to the relatively thin wedge. This resulted in the strain energy being spread more diffusely throughout the beam, rather than being concentrated near the debond front, resulting in a larger cohesive zone [4, 26] and a higher overall strain energy input requirement. While beam thickness is the largest source of this dis- parity, other sources include differences in relative humidity during testing, displacement rate, and delamination front measurement techniques between the two testing methods.In addition, the error for the wedge test was occasionally higher than for the SCB test. One reason for this is the longer cohesive zone. Another reason is the fourth-order dependence of adhesion energy on debond length, c, for the wedge test (1), compared to the second-order dependence for the SCB test (2). The uncertainty in c was ~10%,

for both tests, which resulted in a relative uncertainty in G_c of ~40% for the wedge test, compared with ~20% for the SCB test.

3.2. PA-based Backsheets

Eight modules with PA-based backsheets were retrieved in the present study (Fig. 3). All were from the same manufacturer, and most of them were fielded for similar exposure times (three to six years). While the adhesion energies of six out of the eight are quite similar (between 200-650 J/m^2), there does appear to be a mild negative correlation between adhesion energy and exposure time. The wedge test result for the unexposed module and SCB test result for the 6-year module are the clear exceptions to this. In both of these, however, debonding occurred in the cell-back metallization (CBM), which tended, in general, to produce unusual adhesion energies throughout the study. Correlation between adhesion energy and climatic zone was difficult to establish, because Köppen-Geiger climatic zones contain a number of factors, such as temperature, humidity, and precipitation, that are broadly defined and vary temporally.

In addition to the CBM layer, a number of the backsheets also debonded at the approximate junction of the backsheet outer and core layers. The latter was a common debond location observed in PA-based backsheet coupons in a parallel study on backsheet coupons subjected in indoor accelerated weathering [27]. However, as all of the PA-based backsheets were coextrusions of three PA layers, this was not a well-defined interface, in contrast to laminated backsheets with adhesive layers bonding films of different materials. Nonetheless, the adhesion energies measured in four of the five modules that separated at this location—200-430 J/m^2—are similar in magnitude to the adhesion energy of fresh PA-based backsheet from the indoor-exposure study—approximately 400 J/m^2.

To the authors' knowledge, no studies of adhesion in PA-based backsheets have been published. The lack of reporting is probably due to the impossibility of doing the more common peel test with this material (it becomes brittle upon exposure) and because the failure of interest is typically embrittlement and cracking [28], rather than delamination. Nonetheless, the in-plane cohesive

strength of PA determined here may be related to the through-thickness cohesive strength that characterizes the cracking phenomenon.

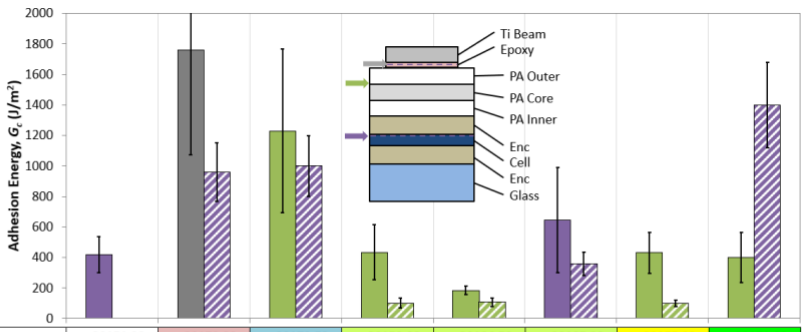

Sample ID	sa30151.32	sa30172.33	sa30173.53	sa30153.23	sa30184.52	sa30185.32	sa30155.23	sa30171.33
Manufacturer	C	C	C	C	C	C	C	C
Location	- Unexp -	AZ, USA	Thailand	China	China	China	Italy	Italy
Climate Zone		BWh	Aw	Cfa	Cfa	Cfa	Csa	Cfb
Exposure (yrs)	0	3	4	4	4.5	5	5	6
Wedge Adh En (J/m²)	418 ± 116	1758 ± 684	1229 ± 538	434 ± 179	184 ± 27	645 ± 347	430 ± 132	400 ± 165
SCB Adh En (J/m²)	Not Tested	>960 ± 192	>1000 ± 200	101 ± 31	107 ± 28	357 ± 77	99 ± 20	>1400 ± 280

Figure 3: Adhesion energies and debond interfaces in field modules with PA-based backsheets. Wedge and SCB results correspond to the solid and hashed columns, respectively. Column color indicates debond interface. (For interpretation of the references to color in this figure, the reader is referred to the online version of this article.)

3.3. PET-based Backsheets

Eight modules with PET-based backsheets were retrieved in the present study (Fig. 4). In contrast to the PA modules, they were produced by several different manufacturers and fielded over a larger range of exposure times (0 to 18 years). Despite the range in exposure times, all seven exposed modules tended to show quite low adhesion energies (8-225 J/m^2) compared to the unexposed module. ,This may be due to the adhesive strength reaching a minimum for these backsheets after only a relatively short amount of field exposure. The parallel study on indoor-exposed backsheets [27] found that the adhesion energy of the PET-based backsheet studied degraded almost to a stable minimum within the first 2000 hours of exposure.

With regard to debond location, the results were quite varied, with no observable correlations with exposure time or climatic zone. The most common locations were the cell-back metallization (CBM), followed by the backsheet outer tie layer. To the authors' knowledge, no studies have been published on adhesion in PET-based backsheets, but studies on other backsheets with tie layers, such as PVDF-based [10] and PVF-based [2, 4, 20], have reported the outer fluoropolymer to tie layer as a common debond interface.

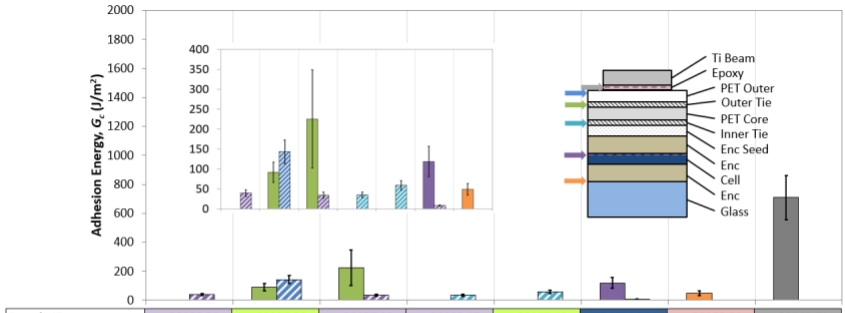

Sample ID	sa30180.33	sa30025.32	sa30177.23	sa30183.25	sa30187.21	sa30175.11	sa30162.31	sa30163.71
Manufacturer	M	H	M	M	H	M	N	R
Deployment Location	CO, USA	OH, USA	CO, USA	CO, USA	Taiwan	CO, USA	AZ, USA	-No Historical
Climate Zone	Bsk	Cfa	Bsk	Bsk	Cfa	Dfb	BWh	Data-
Exposure (yrs)	0	4	6.5	9	10	11	18	
Wedge Adh En (J/m²)	-Not Meas-	91 ± 25	225 ± 123	Not Tested	-Not Meas-	119 ± 38	49 ± 15	708 ± 153
SCB Adh En (J/m²)	40 ± 8	143 ± 30	34 ± 8	35 ± 7	59 ± 12	8 ± 2	Not Tested	Not Tested

Figure 4: Adhesion energies and debond interfaces in field modules with PET-based back- sheets. The inset shows the left-most seven modules, with the abscissa scaled to show relative column heights more clearly.

3.4. PVF-based Backsheets

Modules with PVF-based backsheets were, by far, the most common in this study. The module backsheets all had a PVF outer layer, while the inner layer consisted of either another PVF layer (Fig. 5), an encapsulant seed layer, or another, less common layer (Fig. 6). The core layer typically consisted of PET, but was sometimes a foil, an unidentified, or another PVF layer. From the test results, the most common debond location was the backsheet outer tie layer, which is also the most common reported in the literature [2, 4, 20]. Among Figs. 5 and 6, there is a trend of decreasing adhesion energy with exposure time. For the five 28-year-old modules, while the SCB test was able to capture their adhesion energies, the wedge test was unable to. This was due to the selected wedge beam thickness (0.43 mm) being too high for samples of such weak adhesion, resulting in a relatively stiff beam that pulled off completely during wedge insertion. While a thinner beam could have remedied this problem, the influence of beam stiffness on cohesive zone length and debond length measurement prompted us to maintain a constant beam thickness among

all our tests.

Several studies have reported adhesion energy values for PVF-based backsheets. Previous studies by Novoa, et al [20] and Tracy et al [4] both measured values of approximately 1000 J/m^2 at the "PVF-outer/PET-core interface" in unweathered PVF/PET backsheets. The authors, however, did not specify which exposed surface contained the tie layer or if the tie layer failed cohesively. In addition, Tracy et al [4], were able to measure the adhesion energies of the two 28-year modules from manufacturer A. They found them to have average adhesion energies of 17.4 J/m^2 and 49.4 J/m^2, for the module stored in a shed and the module exposed in the field, respectively. Studies on modules with intermediate exposure times and ageing conditions, comparable to the field-retrieved modules, are difficult to find in the literature.

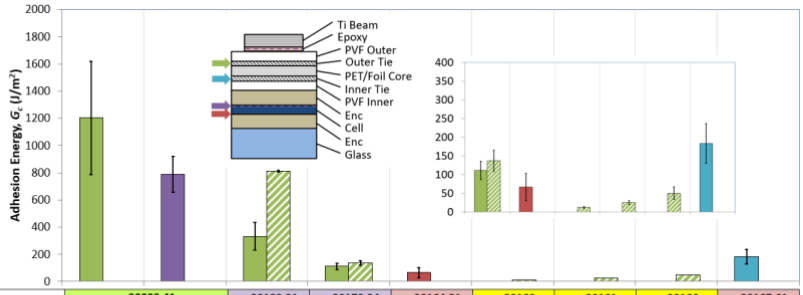

Sample ID	sa30023.41		sa30182.31	sa30179.34	sa30164.21	sa30160	sa30161	sa30166	sa30167.61
Manufacturer	I		F	F	O	A (Shed)	A (Field)	O	L
Deployment Location	OH, USA		CO, USA	CO, USA	AZ, USA	CA, USA	CA, USA	CA, USA	AZ, USA
Climate Zone	Cfa		Bsk	Bsk	BWh	Csa	Csa	Csa	BWh
Exposure (yrs)	4		< 10	10	18	28	28	28	- No Data -
Wedge Adh En (J/m^2)	1204 ± 416	789 ± 130	332 ± 101	111 ± 25	66 ± 37	-Not Meas-	-Not Meas-	-Not Meas-	183 ± 53
SCB Adh En (J/m^2)	Not Tested		812 ± 176	137 ± 28	Not Tested	12 ± 3	25 ± 5	50 ± 16	Not Tested

Figure 5: Adhesion energies and debond interfaces in field modules with PVF-based backsheets, where the inner layer was PVF. The inset shows the right-most six modules, with the abscissa scaled to show relative column heights more clearly.

3.5. PVDF-based Backsheets

The five modules with PVDF-based backsheets tested in this study (Fig. 7) all came from different module manufacturers, although it is not known if the backsheets, themselves, came from the same manufacturer or not. All were fielded for similar lengths of time. The backsheets were comprised of a PVDF

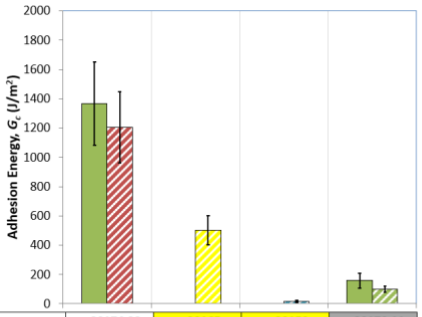

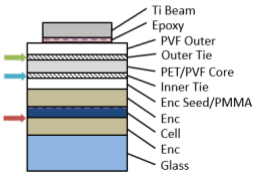

Sample ID	sa30174.32	sa30165	sa30159	sa30170.11
Manufacturer	C	P	K	H
Deployment Location	- Unexp -	CA, USA	CA, USA	-No Historical
Climate Zone		Csa	Csa	Data-
Exposure (yrs)	0	28	28	
Wedge Adh En (J/m²)	1368 ± 284	-Not Meas-	-Not Meas-	158 ± 49
SCB Adh En (J/m²)	1205 ± 242	> 500 ± 100	17 ± 7	99 ± 20

Figure 6: Adhesion energies and debond interfaces in field modules with PVF-based backsheets, where the inner layer was an EVA seed layer (or other)

outer layer and PET core layer, with an optional encapsulant seed layer.

Among the results, there does appear to be a negative correlation between adhesion energy and exposure time, but it is somewhat weak. Of note is the fact that the two modules weathered in dry climatic zones—those from Manufacturers D and E—had higher adhesion energies (approximately 1100 ± 450 J/m^2, averaged between the two) than the remaining three (approximately 250-570 ± 100 J/m^2, averaged between the three) which were weathered in humid climatic zones. More modules would need to be tested to verify this possible correlation, but humidity is well known to correlate with adhesion strength [26].

Almost all of the modules debonded in the outer tie layer. This was a common (in fact, the only) debond location among the PVDF coupons in the parallel indoor exposure study [27], and was the common debond location among other studies on three-layered backsheets with tie layers [2, 4, 20]. Few backsheet ad- hesion studies, however, have focused on this backsheet, specifically. Oreski and Wallner [10], found the adhesion at the "PVDF-outer/PET-core interface" of an unweathered PVDF/PET-based backsheet to be 192 J/m^2, much less than the energy measured in this work, but resulting from a different method (T-peel) and likely a different backsheet manufacturer.

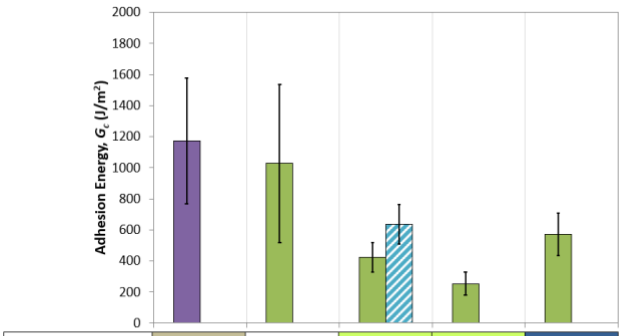

Sample ID	sa30146.42	sa30176.43	sa30035.31	sa30032.33	sa30168.13
Manufacturer	D	E	S	G	C
Deployment Location	AZ, USA	CA, USA	OH, USA	OH, USA	CO, USA
Climate Zone	Csb	Csb	Cfa	Cfa	Dfb
Exposure (yrs)	2	4	4	4	6
Wedge Adh En (J/m²)	1172 ± 404	1027 ± 509	423 ± 94	254 ± 75	571 ± 137
SCB Adh En (J/m²)	Not Tested	Not Tested	635 ± 129	Not Tested	Not Tested

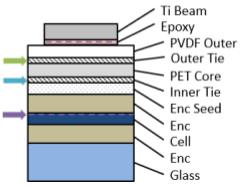

Figure 7: Adhesion energies and debond interfaces in field modules with PVDF-based backsheets.

3.6. FEVE-based Backsheets

The only module with a fluoroethylene vinyl ether (FEVE)-based backsheet in our study demonstrated quite high adhesion energies for both the wedge and SCB tests (Fig. 8). After four years of exposure in a humid, subtropical climate zone (Cfa), debonding within the backsheet was not seen, and occurred, instead, between the Ti test beam and epoxy (wedge test) or between the top EVA and glass (SCB test). It is difficult to draw general conclusions about this backsheet type from this single module, but its high adhesion energy is comparable to the other four-year fluoropolymer-based backsheets weathered in the same location (Figs. 5 and 7). To the authors' knowledge, the present study is the only to test the adhesion of a backsheet of this type.

3.7. THV-based Backsheets

Three tetrafluoroethylene/hexafluoropropylene/vinylidene fluoride co-polymer (THV)-based backsheets were tested in this study (Fig. 9). The two modules from manufacturer "Q" were of identical make and model, with one weathered in the field while the other was not. All three modules had quite low adhesion energies, with adhesion energy decreasing with exposure time.. The authors know of no other fracture mechanics-based adhesion studies have been

conducted on field modules

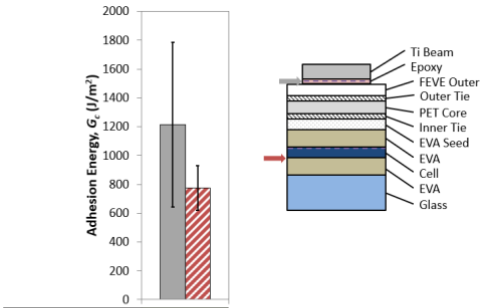

Sample ID	sa30029.42
Manufacturer	B
Deployment Location	OH, USA
Climate Zone	Cfa
Exposure (yrs)	4
Wedge Adh En (J/m²)	1214 ± 570
SCB Adh En (J/m²)	774 ± 155

Figure 8: Adhesion energies and debond interfaces in field module with FEVE-based back-sheets.

with this backsheet type. .

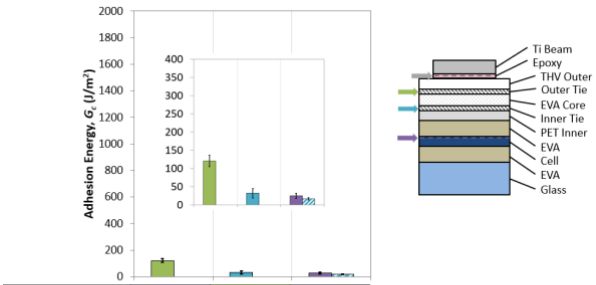

Sample ID	sa30181.31	sa30020.43	sa30178.34
Manufacturer	Q	J	Q
Deployment Location	CO, USA	OH, USA	CO, USA
Climate Zone	Bsk	Cfa	Bsk
Exposure (yrs)	0	4	5.5
Wedge Adh En (J/m²)	121 ± 16	32 ± 13	25 ± 7
SCB Adh En (J/m²)	-Not Meas-	Not Tested	17 ± 4

Figure 9: Adhesion energies and debond interfaces in field modules with THV-based back-sheets. The inset shows all three modules, with the abscissa scaled to show relative column heights more clearly.

3.8. Trends Among Climatic Zone or Exposure Time

While there was an observable trend of decreasing adhesion energy with increasing exposure time for five out of the six backsheet types, in general it was difficult to observe any trends between adhesion energy and climatic zone. This is likely because of the broad ranges of temperature, humidity, and precipitation that define Köppen-Geiger climatic zones, as well as the wide range of variations in backsheet film and adhesive compositions that can exist from module to module. Even for modules with the same nominal backsheet type, same climatic zone, and same exposure time, the differences in specific backsheet composition; local differences in cli- matic conditions within the same climatic zone; installation configurations such as roof vs. rack; and differences in tilt angle, rack height, and ground cover; can all cause variations in degradation.

3.9. Trends Among Backsheets with Field Delamination

It is informative to compare the adhesion energies of modules that did and did not exhibit backsheet delamination during field exposure. Fig. 10 shows this for all of the SCB-tested modules that separated in the backsheet or cell-back metallization during testing. Here, backsheet delamination is defined as the presence of visible bubbles or separation between layers of the backsheet, when the module was deployed in the field. The delamination could have occurred between the layers of the backsheet, or between the backsheet and the backside of the module. Of the thirty-seven modules tested in this study, five exhibited field delamination. These five had low adhesion energy, and, while the SCB test was able to measure all five, the wedge test was not, due to complete delamination during initial insertion of the beam (c.f. Section 3.4).

The data in Fig. 10 shows that the majority of the modules were fielded for ten years or less, with the exception of the five 28-year modules. Among the modules, all whose backsheet had an adhesion energy greater than ~100 J/m^2 exhibited no field delamination. This suggests an upper threshold for measured adhesion energy which modules can be expected to show no delamination in the field. A single module below 10

J/m^2 was also found to exhibit field delamination suggesting a lower limit below which any material is likely to fail. These results are consistent with other reported values [5].

The above results have the potential of enabling prediction of backsheet delamination, based upon the results of adhesion tests. One could envision a backsheet qualification adhesion test where stresses believed to equate to roughly 10 years or a lifetime are applied, and a result is considered passing if the strength is greater than 100 J/m^2. While this would err on the side of producing false negatives, a conservative approach like this is justified because the cost difference between alternative backsheet

materials is not significant relative to the whole cost of a PV system.

Figure 10: Comparison of all SCB-tested modules with and without field delamination. The dashed line at ~100 J/m^2 is a suggested threshold, above which no modules exhibited field delamination..

4. Conclusion

In the present work, two methods were employed to measure the adhesion energy of modules exposed in the field: the wedge test and the width-tapered single cantilever beam (SCB) test. Thirty-seven modules were tested, encompassing six different backsheet outer layer polyer classes: PA, PET, PVF, PVDF, FEVE, and THV. Among the modules within each polymer class, adhesion energy tended to decrease with exposure time. Debond location, on the other hand, was typically quite varied, with generally no clear correlation with exposure time or climatic zone. Among the modules with PET-, PVF- and PVDF-based backsheets, the most common debond location within the backsheet was the outer tie layer. This matches literature trends among field-exposed and indoor-weathered backsheets with tie layers [2, 4, 10, 20]. Among the modules with PA-based backsheets, the debonding was cohesive in nature and often occurred near the junction of the outer and core PA layers. While cracking, rather than delamination, is more commonly observed in the field [28], the in-plane cohesive strength determined, herein, may be useful for understanding through-thickness cracking.

A comparison of modules that did and did not exhibit field delamination in the backsheet showed that those with SCB-measured adhesion energies higher than ~100 J/m^2 exhibited no field delamination. This threshold may potentially serve as the basis for adhesion qualification tests for backsheets.

Between the two testing methods, the wedge test tended to produce slightly higher mean adhesion energies and slightly larger error. While the greater error is inherent to the method, the disparity in means is not always statistically significant, and it could

potentially be mitigated by more closely controlling in situ humidity, and by adjusting testing parameters such as beam thickness, wedge insertion rate, dwell time, and crack length measurement technique. Therefore, since the wedge test is simpler to set up, it could be used when convenience is desired, at the expense of slightly higher uncertainty. On the other hand, the SCB test could be used when lower uncertainty is desired, and time and resources allow for a slightly more complex test setup.

Ultimately, the two methods employed in the present study provide alternative means of measuring the adhesion energy in backsheets. Furthermore, the broad range of modules and backsheets tested serve as a basis for establishing future correlations between accelerated tests and outdoor field degradation. Such work is critical if backsheets are to perform their intended function throughout their 25-year (or greater) service lives.

Acknowledgments

This work was supported by the Department of Energy, Office of Energy Efficiency and Renewable Energy (EERE), "Physics of Reliability: Evaluating Design Insights for Component Technologies in Solar 2" (PREDICTS2) project, award no. DE-EE0007143. In addition to the contributions of the authors, grateful acknowledgement is extended to the following individuals for their contributions: Nick Bosco for helpful instruction on the implementation of the SCB test. David C. Miller at NREL, for providing additional material samples and experimental direction; Tiange Zhan, Jianfeng Sun, Kaizhen Zhang, Bran- don Ho, Amanda Cheung, and Brian Liang, at Northeastern University, for their help with the experimental work.

Disclaimer

This work was authored, in part, by the National Renewable Energy Laboratory, operated by Alliance for Sustainable Energy, LLC, for the U.S. Department of Energy (DOE) under Contract No. DE-AC36-08GO28308, and in part by the National Institute of Standards and Technology. Neither the United States Government nor any agency thereof, nor any of their employees, makes any warranty, express or implied, or assumes any legal liability or responsibility for the accuracy, completeness, or usefulness of any information, apparatus, product, or process disclosed, or represents that its use would not infringe privately owned rights. The views and opinions of authors expressed herein do not necessarily state or reflect those of the United States Government or any agency thereof. Certain commercial equipment, instruments, or materials are identified in this work in order to adequately detail the experimental procedure. Such identification is not intended to imply recommendation or endorsement by the National Institute of Standards and Technology, the United States Government, or any agency thereof, nor is it intended to imply that the materials and equip- ment identified are necessarily the best available for this purpose. The U.S. Government retains and the publisher, by accepting the article for publication,

References

[1] M. Quintana, D. King, T. McMahon, C. Osterwald, Commonly observed degradation in field-aged photovoltaic modules, in: Conference Record of the Twenty-Ninth IEEE Photovoltaic Specialists Conference, 2002., IEEE, 2002, pp. 1436–1439. doi:10.1109/PVSC.2002.1190879.

[2] P. Sánchez-Friera, M. Piliougine, J. Pelaez, J. Carretero, M. Sidrach de Cardona, Analysis of degradation mechanisms of crystalline silicon pv modules after 12 years of operation in southern europe, Progress in photovoltaics: Research and Applications 19 (6) (2011) 658–666. doi:10.1002/pip.1083.

[3] W. Gambogi, Y. Heta, K. Hashimoto, J. Kopchick, T. Felder, S. MacMaster, A. Bradley, B. Hamzavytehrany, L. Garreau-Iles, T. Aoki, et al., A comparison of key pv backsheet and module performance from fielded module exposures and accelerated tests, IEEE Journal of Photovoltaics 4 (3) (2014) 935–941. doi:10.1109/JPHOTOV.2014.2305472.

[4] J. Tracy, N. Bosco, F. Novoa, R. Dauskardt, Encapsulation and backsheet adhesion metrology for photovoltaic modules, Progress in Photovoltaics: Research and Applications 25 (1) (2017) 87–96. doi:10.1002/pip.2817.

[5] N. Bosco, J. Eafanti, S. Kurtz, J. Tracy, R. Dauskardt, Defining threshold values of encapsulant and backsheet adhesion for pv module reliability, in: 2017 IEEE 44th Photovoltaic Specialist Conference (PVSC), IEEE, 2017, pp. 3190–3194. doi:10.1109/PVSC.2017.8366641.

[6] J. Tracy, D. R. D'hooge, N. Bosco, C. Delgado, R. Dauskardt, Evaluating and predicting molecular mechanisms of adhesive degradation during field and accelerated aging of photovoltaic modules, Progress in Photovoltaics:

Research and Applications 26 (12) (2018) 981–993. doi:10.1002/pip.3045.

[7] ASTM D1876 Standard Test Method for Peel Resistance of Adhesives (T-Peel Test), Standard, ASTM International, West Conshohocken, PA, USA (2015). doi:10.1520/D1876-08R15E01.

[8] ASTM D6862 Standard Test Method for 90 Degree Peel Resistance of Adhesives, Standard, ASTM International, West Conshohocken, PA, USA (2016). doi:10.1520/D6862-11R16.

[9] ASTM D903 Standard Test Method for Peel or Stripping Strength of Adhesive Bonds, Standard, ASTM International, West Conshohocken, PA, USA (2017). doi:10.1520/D0903-98R17.

[10] G. Oreski, G. Wallner, Delamination behaviour of multi-layer films for pv encapsulation, Solar energy materials and solar cells 89 (2-3) (2005) 139–151. doi:10.1016/j.solmat.2005.02.009.

[11] G. Jorgensen, K. Terwilliger, J. DelCueto, S. Glick, M. Kempe, J. Pankow, F. Pern, T. McMahon, Moisture transport, adhesion, and corrosion protection of pv module packaging materials, Solar Energy Materials and Solar Cells 90 (16) (2006) 2739–2775. doi:10.1016/j.solmat.2006.04.003.

[12] F. Pern, S. Glick, Adhesion strength study of eva encapsulants on glass substrates, Tech. rep., National Renewable Energy Lab.(NREL), Golden, CO (United States) (2003).

[13] F.-J. Pern, G. J. Jorgensen, Enhanced adhesion of eva laminates to primed glass substrates subjected to damp heat exposure, in: Conference Record of the Thirty-first IEEE Photovoltaic Specialists Conference, 2005., IEEE, 2005, pp. 495–498. doi:10.1109/PVSC.2005.1488178.

[14] M. D. Kempe, G. J. Jorgensen, K. M. Terwilliger, T. J. McMahon, C. E. Kennedy, T. T. Borek, Acetic acid production and glass transition concerns

with ethylene-vinyl acetate used in photovoltaic devices, Solar Energy Materials and Solar Cells 91 (4) (2007) 315–329. doi:10.1016/j.solmat.2006.10.009.

[15] ASTM D1002 Standard Test Method for Apparent Shear Strength of Single-Lap-Joint Adhesively Bonded Metal Specimens by Tension Loading (Metal-to-Metal), Standard, ASTM International, West Conshohocken, PA, USA (2019). doi:10.1520/D1002-10R19.

[16] V. Chapuis, S. Pélisset, M. Raeis-Barnéoud, H.-Y. Li, C. Ballif, L.-E. Perret-Aebi, Compressive-shear adhesion characterization of polyvinyl-butyral and ethylene-vinyl acetate at different curing times before and after exposure to damp-heat conditions, Progress in Photovoltaics: Research and Applications 22 (4) (2014) 405–414. doi:10.1002/pip.2270.

[17] D. King, M. Quintana, J. Kratochvil, D. Ellibee, B. Hansen, Photovoltaic module performance and durability following long-term field exposure, Progress in Photovoltaics: Research and Applications 8 (2) (2000) 241–256. doi:10.1002/(SICI)1099-159X(200003/04)8:2<241::AID-PIP290>3.0.CO;2-D.

[18] M. Quintana, D. King, F. Hosking, J. Kratochvil, R. Johnson, B. Hansen, N. Dhere, M. Pandit, Diagnostic analysis of silicon photovoltaic modules after 20-year field exposure, in: Conference Record of the Twenty-Eighth IEEE Photovoltaic Specialists Conference-2000 (Cat. No. 00CH37036), IEEE, 2000, pp. 1420–1423. doi:10.1109/PVSC.2000.916159.

[19] S. R. Dupont, M. Oliver, F. C. Krebs, R. H. Dauskardt, Interlayer adhesion in roll-to-roll processed flexible inverted polymer solar cells, Solar Energy Materials and Solar Cells 97 (2012) 171–175. doi:10.1016/j.solmat.2011.10.012.

[20] F. D. Novoa, D. C. Miller, R. H. Dauskardt, Environmental mechanisms of debonding in photovoltaic backsheets, Solar Energy Materials and Solar Cells 120 (2014) 87–93. doi:10.1016/j.solmat.2013.08.020.

[21] F. D. Novoa, D. C. Miller, R. H. Dauskardt, Adhesion and debonding kinetics of photovoltaic encapsulation in moist environments, Progress in Photovoltaics: Research and Applications 24 (2) (2016) 183–194. doi: 10.1002/pip.2657.

[22] M. Kempe, J. Wohlgemuth, D. Miller, L. Postak, D. Booth, N. Phillips, Investigation of a wedge adhesion test for edge seals, in: Reliability of Photovoltaic Cells, Modules, Components, and Systems IX, Vol. 9938, International Society for Optics and Photonics, 2016, p. 993803. doi: doi.org/10.1117/12.2239161.

[23] T. L. Anderson, Fracture mechanics: fundamentals and applications, CRC press, 2005.

[24] M. Gilliam, Polymer surface treatment and coating technologies, Handbook of Manufacturing Engineering and Technology (2015) 99–124doi:10.1007/978-1-4471-4670-4_20.

[25] IEC DTS 62788-6-3 Ed. 1: Measurement procedures for materials used in photovoltaic modules - Adhesion testing of interfaces within PV modules, Standard, International Electrotechnical Commission, Geneva, Switzerland (2018).

[26] N. Bosco, J. Tracy, R. Dauskardt, Environmental influence on module delamination rate, IEEE Journal of Photovoltaics 9 (2) (2018) 469–475. doi:10.1109/JPHOTOV.2018.2877436.

[27] S. E. Julien, M. D. Kempe, J. J. Eafanti, J. Morse, Y. Wang, A. Fairbrother, S. Napoli, A. W. Hauser, L. Ji, G. S. O'Brien, X. Gu, R. H. French, K. P. Boyce, L. S. Bruckman, K. T. Wan, Characterizing photovoltaic backsheet adhesion degradation using the wedge and single cantilever beam tests, part ii: Accelerated tests, In Review.

[28] A. Fairbrother, S. Julien, K.-T. Wan, L. Ji, K. Boyce, S. Merzlic, A. Lefebvre, G. O'Brien, Y. Wang, L. Bruckman, et al., Degradation analysis

of field-exposed photovoltaic modules with non-fluoropolymer-based back-sheets, in: Reliability of Photovoltaic Cells, Modules, Components, and Systems X, Vol. 10370, International Society for Optics and Photonics, 2017, p. 1037003. doi:10.1117/12.2272488.

Supplemental Information

SI Table 1: Detailed module characteristics.

SampleID	Make	Exposure Location	Climatic Zone	Ground Cover	Exposure Year	Outer layer	Core layer	Inner layer	Notes
sa30151	C	Unexposed				PA	PA+PP+glass fiber	PA	
sa30153	C	Changshu, China	Cfa	concrete roof	4	PA	PA+PP+glass fiber	PA	
sa30155	C	Rome, Italy	Csa	grass	5	PA	PA+PP+glass fiber	PA	
sa30171	C	Bergamo, Italy	Cfa	grass	6	PA	PA+PP+glass fiber	PA	
sa30172	C	Tonopah, AZ, US	BWh	dirt	3	PA	PA+PP+glass fiber	PA	
sa30173	C	Thailand	Aw	grass	4	PA	PA+PP+glass fiber	PA	
sa30184	C	Changshu, China	Cfa	concrete roof	5	PA	PA+PP+glass fiber	PA	
sa30185	C	Changshu, China	Cfa	grass	6	PA	PA+PP+glass fiber	PA	
sa30186	C	Changshu, China	Cfa	grass	6	PA	PA+PP+glass fiber	PA	
sa30190	C	Changshu, China	Cfa	concrete roof	5	PA	PA+PP+glass fiber	PA	
sa30187	H	Taiwan	Cfa	concrete roof	10	PET (clear)	PET (white)	EVA (white)	
sa30175	M	Westminster, CO, US	BSk	gap	11	PET (clear)	PET (white)	EVA	
sa30177	M	Lakewood, CO, US	BSk	white roof	6.5	PET (clear)	PET (white)	EVA	
sa30180	M	Lakewood, CO, US	BSk	dirt	0	PET (clear)	PET (white)	EVA	
sa30183	M	Denver, CO, US	BSk	dirt	9.25	PET (clear)	PET (white)	EVA	
sa30191	M	Broomfield, CO, US	BSk	rock	9	PET (clear)	PET (white)	EVA	Field survey data, not retrieved
sa30162	N	Arizona	BWh	dirt	18	PET (clear)	PET (white)	EVA	
sa30163	R	NA	NA	NA	NA	PET			No exposure information
sa30025	H	Cleveland, OH, US	Cfa	grass	4	PET (white)	PET (clear)	EVA	
sa30160	A	SMUD, CA, US	Csa	dirt	28 or 0?	PVF	PET	PVF	store in shed
sa10161	A	SMUD, CA, US	Csa	dirt	28	PVF	PET	PVF	
sa30174	C	Unexposed			0	PVF	PET	EVA	
sa30179	F	Lakewood, CO, US	BSk	dirt	10.3	PVF			
sa30182	F	Lakewood, CO, US	BSk	dirt	10.3	PVF			
sa30170	H					PVF	PVF	EVA	no exposure information
sa30159	K	SMUD, CA, US	Csa	dirt	28	PVF			outer layer delamination
sa30167	L					PVF			no exposure information
sa30164	O	Mesa, AZ, US	BWh	dirt	18	PVF	?	PVF	
sa30166	O	SMUD, CA, US	Csa	dirt	28	PVF	PET	PVF	
sa30165	P	SMUD, CA, US	Csa	dirt	28	PVF	?	PMMA	
sa30023	I	Cleveland, OH, US	Cfa	grass	4	PVF	PET	PVF	
sa30176	E	San Jose, CA, US	Csb	dirt	3.75	PVDF (alpha phase, with acrylic)	PET		
sa30032	G	Cleveland, OH, US	Cfa	grass	4	PVDF (alpha phase, without acrylic)	PET		
sa30168	C	Golden, Colorado, US	BSk	dirt	6	PVDF (beta phase, with acrylic)	PET		
sa30146	D	Arizona, Flagstaff, US	Csb	dirt	2	PVDF (beta phase, with acrylic)	PET		
sa30035	S	Cleveland, OH, US	Cfa	grass	4	PVDF (beta phase, with acrylic)	PET		
sa30029	B	Cleveland, OH, US	Cfa	grass	4	FEVE			
sa30023	J	Cleveland, OH, US	Cfa	grass	4	THV			
sa30178	Q	Lakewood, CO, US	BSk	dirt	6.5	THV			
sa30181	Q	Lakewood, CO, US	BSk	dirt	0	THV			

[i] Adhesion and debonding kinetics of photovoltaic encapsulation in moist environments Fernando D. Novoa[1], David C. Miller[2] and Reinhold H. Dauskardt[1]*